Supplementary Information:

Symmetry-breaking dynamics of a photoionized carbon dioxide dimer

Author list: Ester Livshits,[1,2] Dror M. Bittner,[1] Florian Trost,[3] Severin Meister,[3] Hannes Lindenblatt,[3] Rolf Treusch[4], Krishnendu Gope,[1,5] Thomas Pfeifer,[3] Roi Baer,[1,2] Robert Moshammer,[3] Daniel Strasser[1*]

Affiliations:

[1]Institute of Chemistry, The Hebrew University of Jerusalem, Jerusalem, Israel

[2]Fritz Haber Research Center of Molecular Dynamics, The Hebrew University of Jerusalem, Jerusalem, Israel

[3]Max Planck Institute for Nuclear Physics, Heidelberg, Germany

[4]Deutsches Elektronen-Synchrotron DESY, Hamburg, Germany.

[5]IISER-Thiruvananthapuram, Vithura, Kerala-695551, India

* Corresponding authors: Daniel Strasser strasser@huji.ac.il

Roi Baer roi.baer@huji.ac.il

Supplementary Note 1: EUV photon energy dependence

Supplementary Figure 1 shows the measured KER spectrum as a function of photon energy. The measurement is performed at a fixed 500fs time delay between the EUV pump and EUV probe pulses. The total yield of $CO_2^+ + CO_2^+$ coincidences increases with photon energy. Nevertheless, the shape of the KER spectrum remains the same. In particular the presence of the KER tails, above and below the narrow ~ 3.8 eV KER peak observed at the t=0 fs delay (shown in figure 1 of the main text). We conclude that the reported EUV pump – EUV probe signal is not specific to a particular resonant excitation or to excitation above the single-photon double ionization threshold supporting its interpretation as Coulomb explosion due to a sequential 1st photoionization and 2nd ionization events.

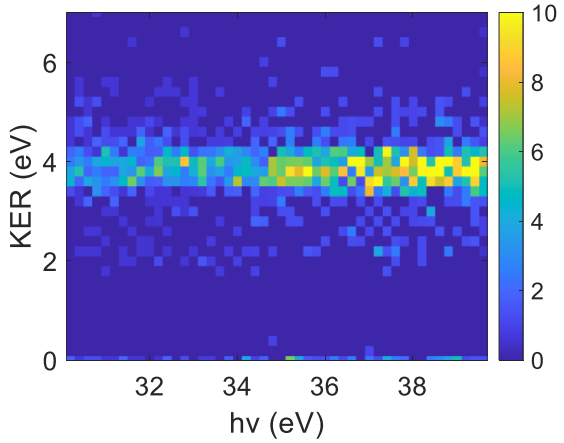

Supplementary Figure 1, shows the KER spectrum of coincident pairs of CO_2^+ ions as a function of photon energy. Colormap indicates the relative yield of measured events. The time delay is kept fixed at 500 fs and exhibits the same KER spectrum shape shown in figure 1 of the main manuscript for 39 eV photons. Source data are provided as a Source Data file.

Supplementary Note 2: EUV pump – EUV probe time-response function

The interpretation of the measured time dependence requires an estimate of the experimental time-response function that depends on the time duration of the FEL pulses as well as on the geometrical overlap of the pump and probe pulses in the interaction region with the molecular beam. Supplementary figure 2 shows a simultaneously measured upper limit estimate for the experimental pump-probe time-response function. The KER spectrum of triple $O^+ + C^+ + O^+$ coincidence peaks above 20 eV. The data points in Supplementary figure 3 show the appearance of such triple-coincidences with a total KER within the 10-20 eV window.

We interpret the time dependence as Coulomb explosion initiated by double-ionization of a CO_2 monomer during the pump pulse, followed by a time delayed 3rd ionization during the probe pulse. The response of the signal is therefore expected to be on the time scale of the Coulomb explosion itself, convoluted with the experimental response. Thus, the fitted Gaussian response shown by the blue curve provides an upper σ_t~33±8 fs limit estimate of the experimental time resolution, recorded simultaneously with the CO_2 dimer data.

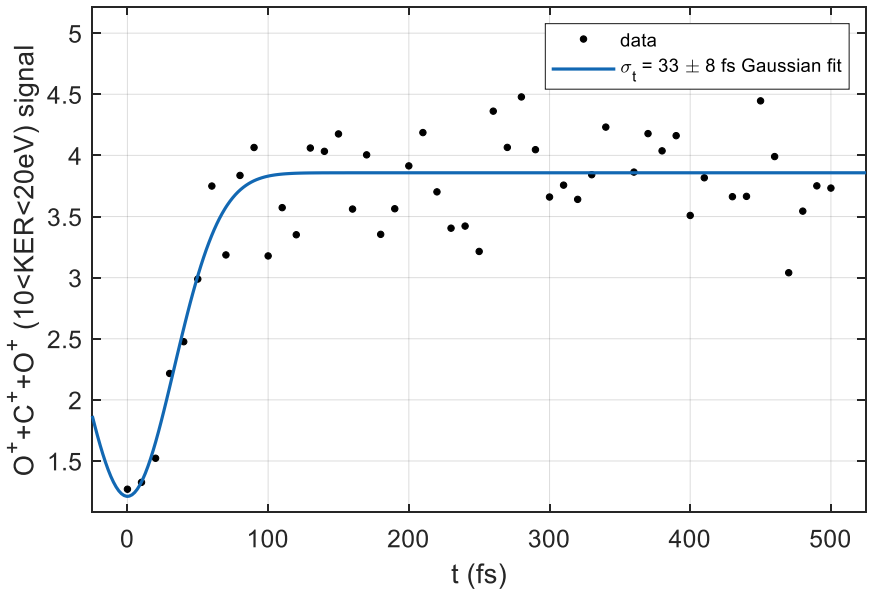

Supplementary Figure 2, shows the time resolved yield of triple-coincidence signal attributed to the CO_2 monomer. The rise of the signal is fitted with a σ_t~33±8 fs Gaussian, providing an upper limit estimate for the experimental time resolution. Source data are provided as a Source Data file.

Supplementary Note 3: Systematic test of the simulated Coulomb explosion KER estimates

The time resolved Coulomb explosion simulations reported in the manuscript were performed by propagating the dications formed by the photoionization probe on the triplet ground-state of the dication using a DFT/BNL potential. Supplementary Figure 3 compares the time-resolved KER of a specific trajectory, which is propagated on the CASPT2 level on the singly ionized ground state, probed on three different dication potentials. The red and blue symbols compare BNL and CASPT2 calculations on the triplet dication ground state. The nearly identical KER traces validate the use of the computationally less expensive method.

Furthermore, the green symbols indicate that also probing by Coulomb explosion on the singlet dication ground-state exhibits a similar trend, in which the KER begins to increase at ~ 100 fs pump-probe delay and falls below the initial level after ~200 fs delay. In this particular trajectory, the KER remains low throughout the simulated 500 fs. Similar comparison was performed for validating the reported stability of metastable $C_2O_4^{2+}$ that are predicted to form after initial population of the 2nd excited state and a time delayed 2nd ionization.

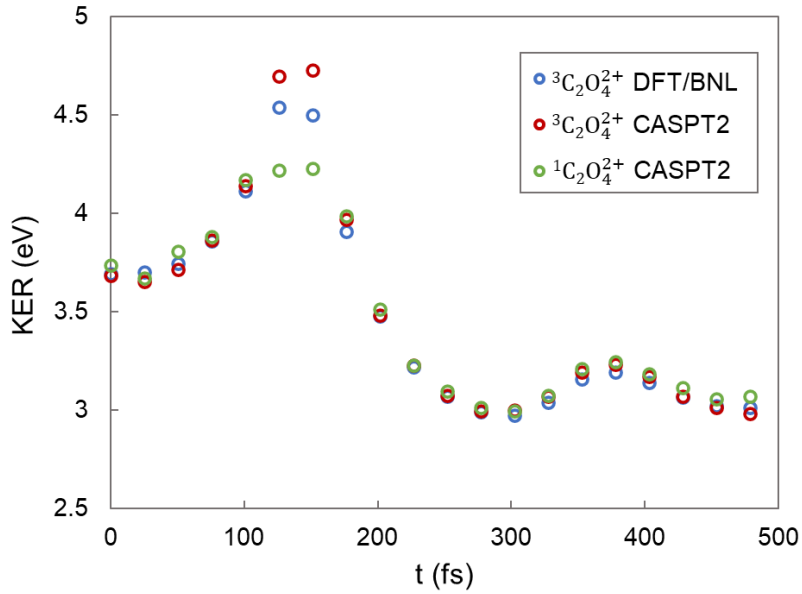

Supplementary Figure 3 compares three different methods for simulating the KER in the $CO_2^+ + CO_2^+$ Coulomb explosion. The simulated KER is shown as a function of the probe 2nd ionization time after the initial ionization by the EUV pump pulse to the dimer cation CASPT2 ground state. Source data are provided as a Source Data file.

Supplementary Note 4: Electronic structure of the CO_2 dimer at the cation global minimum geometry

Figure 2 in the main text showed that 4-state averaged CASPT2 breaks C_{2h} symmetry at the Franck-Condon (FC) geometry of the ionized dimer, while the DFT/BNL calculation does not. Such a symmetry breaking can happen only if there is a degeneracy between B_u and A_g states or B_g and A_u states. Evidence for this degeneracy is the small DFT/BNL gap between the B_u and A_g (or A_u and B_g) states. For example, in Supplementary Figure 4, at the FC geometry, the CASPT2 Dyson orbital is similar in shape to the sum of the nearly degenerate B_u and A_g DFT/BNL orbitals. However, at the global minimum (GM) geometry the situation is different. Here CASPT2 does not break symmetry because the B_u and the A_g states have a large energy gap and therefore, they cannot mix to produce a localized charge state.

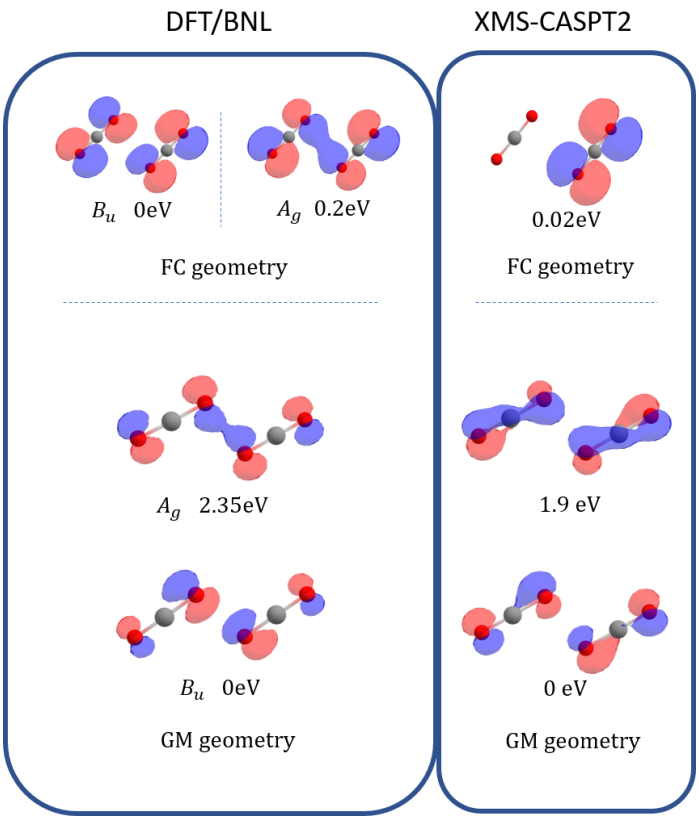

Supplementary Figure 4 compares the electronic structure of the CO2 dimer at two geometries: The Frank-Condon geometry and the global minimum of the singly ionized cation. On the left-hand side we plot DFT/BNL/aug-cc-pvdz occupied A_g and B_u orbitals of the neutral dimer (the DFT/BNL states) and the ionization energies (relative to the ionization energy of the HOMO, taken as zero). On the right-hand side we plot Dyson orbital of the lowest-energy many-body eigenstates within the SA4-XMS-CASPT2(7e6o)/aug-cc-pvdz theory and show the excitation energies relative to the cation ground-state. Source data are provided as a Source Data file.

Supplementary Note 5: Symmetry-Breaking at the Franck-Condon point of the cation CO_2 dimer

In Figure 2, we compared the four states of the SA4-XMS-CASPT2(7e6o) calculation with eight states from DFT. The former were localized and had a shape that was similar to the sum of the two delocalized states of the latter. The SA4-XMS-CASPT2(7e6o) has a limited active space and cannot account for the "missing" four states. Due to limited computational resources, we are not able to perform calculations with eight states in the SA. This is too challenging even in CASSCF (without the PT2 correction). However, we are able to check what happens when six states are included in the SA. For this goal we performed a calculation at the SA6-XMS-CASPT2(17e11o) level and compare the results with those of SA4-XMS-CASPT2(7e6o) in Supplementary Table 1. The leading configurations found by the SA4 calculations are shown on the right. Each having six orbitals, three of which are doubly-occupied, one singly-occupied (this is the "hole" caused by ionization) and the last two unoccupied. On the left we show the configurations found by the SA6 calculation. These have five additional occupied orbitals and when these are doubly occupied the configurations are very similar to those of the SA4 calculation on the right: 22222-222axx of SA6 is analogous to 222axx of SA4, 22222-22a2xx is analogous to 22a2xx etc. The two additional states of the SA6 calculation are those where the hole occupies one of the five orbitals that go beyond the CAS of the SA4 calculation: 2222a-2222xx and 222a2-2222xx. These states have

no analog in the SA4 calculation and it is visually evident that 2222a-2222xx is the “missing sibling” of 22222-222axx and, similarly, 222a2-2222xx is the “missing sibling” of 22222-22a2xx. Furthermore, each of two sibling-states have very similar energies and they are localized on the opposite monomer. We expect that the missing siblings of 2a22xx and a222xx would be recovered in an appropriate SA8 calculation, which is computationally beyond our capability. The overall picture is that the SA4 calculation brings one localized representative from each pair of degenerate states. We expect that the forces on the nuclei are not affected by the symmetry induced degeneracy. In conclusion, we have given indication that the SA4-XMS-CASPT2(7e6o) electronic structure, which is used throughout this study, is qualitatively resilient to improvements in the level of the CAS calculation. It gives a broken-symmetry solution to the electronic structure in a condition of degeneracy.

Supplementary Table 1: Comparison of the SA6 and SA4 CASPT2 calculations at the FC geometry. The leading configuration for each excited state is shown along with a graphic depiction of the hole (singly-occupied) orbital. The weight of the leading configurations is greater than 0.9 in all states shown here. Source data are provided as a Source Data file.

SA6-XMS-CASPT2(17e11o)			SA4-XMS-CASPT2(7e6o)		
Δ E (eV)	Leading Config.	Hole orbital	Hole orbital	Leading Config.	ΔE (eV)
0.00	22222 222axx	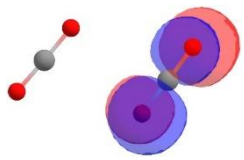	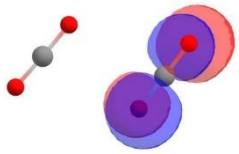	222axx	0.00
0.00	22222 22a2xx	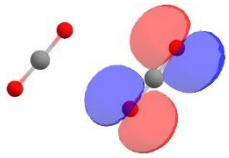	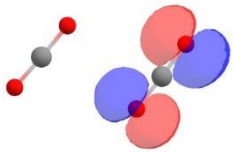	22a2xx	0.02
0.75	2222a 2222xx	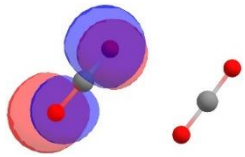			
0.75	222a2 2222xx	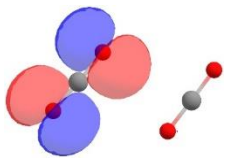			
4.44	22222 2a22xx	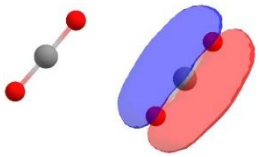	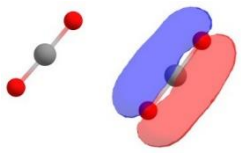	2a22xx	3.63
4.47	22222 a222xx	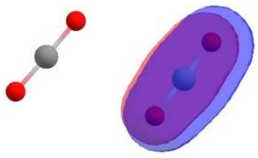	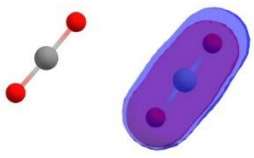	a222xx	3.73

Supplementary Note 6: Systematic test of the symmetric response to positive and negative time delays

As the FEL pulse is split into two equal parts, the response is expected to be symmetric with respect to positive and negative time delays. Supplementary Figure 5 shows the measured KER as a function time, demonstrating the symmetric response in negative and positive times. Note the appearance of high KER events at ~+/- 100 fs and of low KER events at ~ +/- 250 fs appears at both positive and negative time delays. Thus confirming the t=0 assignment and justifying combining the statistics of positive and negative time delays shown in the symmetrized figure 5 in the main text.

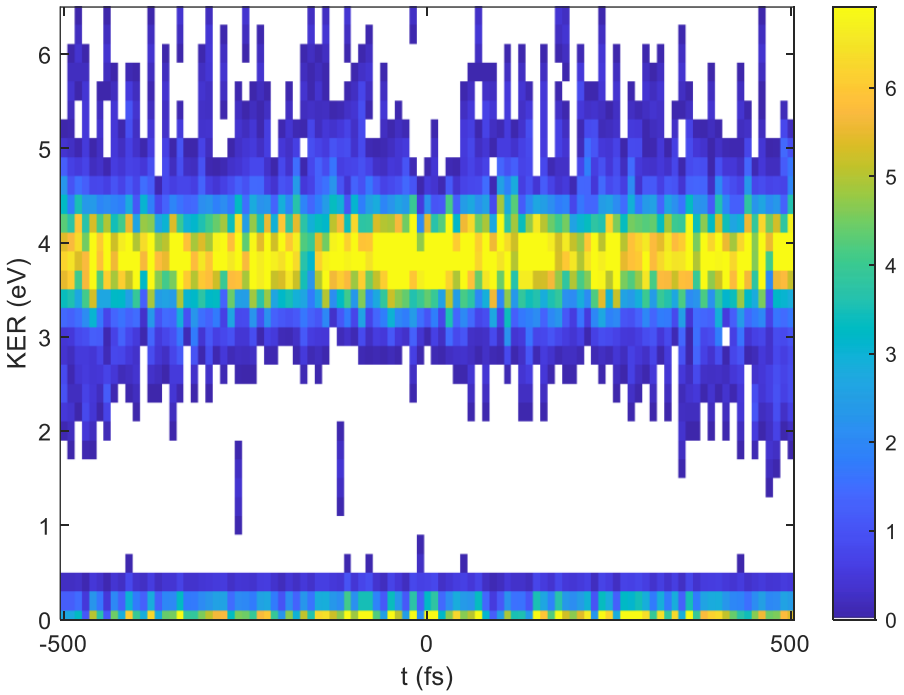

Supplementary Figure 5 Shows the symmetric response of the measured KER for positive vs. negative time delays between the two equal halves of the FEL pulse. Source data are provided as a Source Data file.

Supplementary Note 7: Detailed description of the active space used in the calculations

For completeness, Supplementary Figures 6 and 7 show the active space orbitals for the XMS-CASPT2(7e6o) and XMS-CASPT2(17e11o), respectively, calculated at the first point of the typical trajectory used in all other figures showing orbitals at the FC geometry. The orbitals at this geometry are visually indistinguishable from those calculated at the two following relaxed geometries of the neutral dimer:

1) C2h symmetry-imposed BNL relaxation on the neutral dimer
2) CASPT2 relaxation of the neutral dimer, starting from the C2h symmetry-imposed geometry

The cartesian coordinates (Å) of the three considered FC geometries are:

	Typical trajectory			BNL-relaxed (C2h)			CASPT2-relaxed		
C	1.75	-0.24	0.00	1.70	-0.28	0.00	1.71	0.20	0.00
O	2.45	0.69	0.03	2.47	0.58	0.00	2.46	-0.70	0.00
O	1.02	-1.17	-0.03	0.93	-1.14	0.00	1.00	1.15	0.00
C	-1.72	0.29	0.05	-1.70	0.28	0.00	-1.73	-0.22	0.00
O	-0.98	1.19	0.12	-0.93	1.14	0.00	-0.99	-1.14	0.00
O	-2.50	-0.58	-0.08	-2.47	-0.58	0.00	-2.46	0.70	0.00

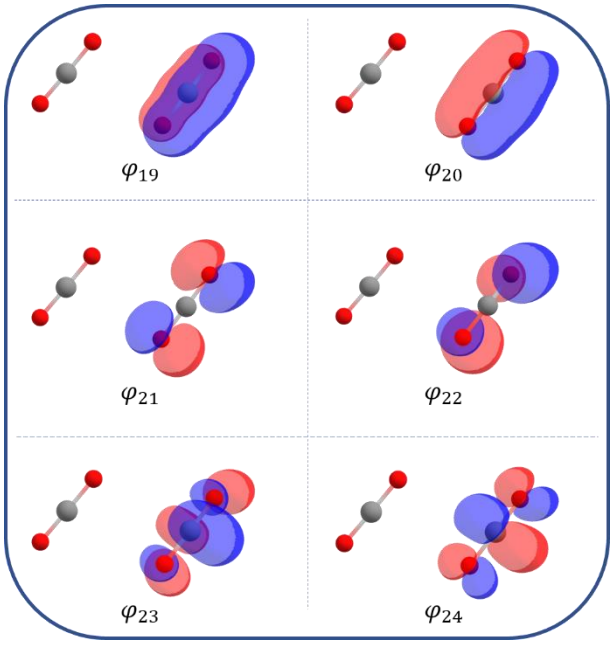

Supplementary Figure 6 Shows the six active XMS-CASPT2(7e6o) orbitals of $(CO_2)_2^+$ at the Franck-Condon (FC) geometry. Source data are provided as a Source Data file.

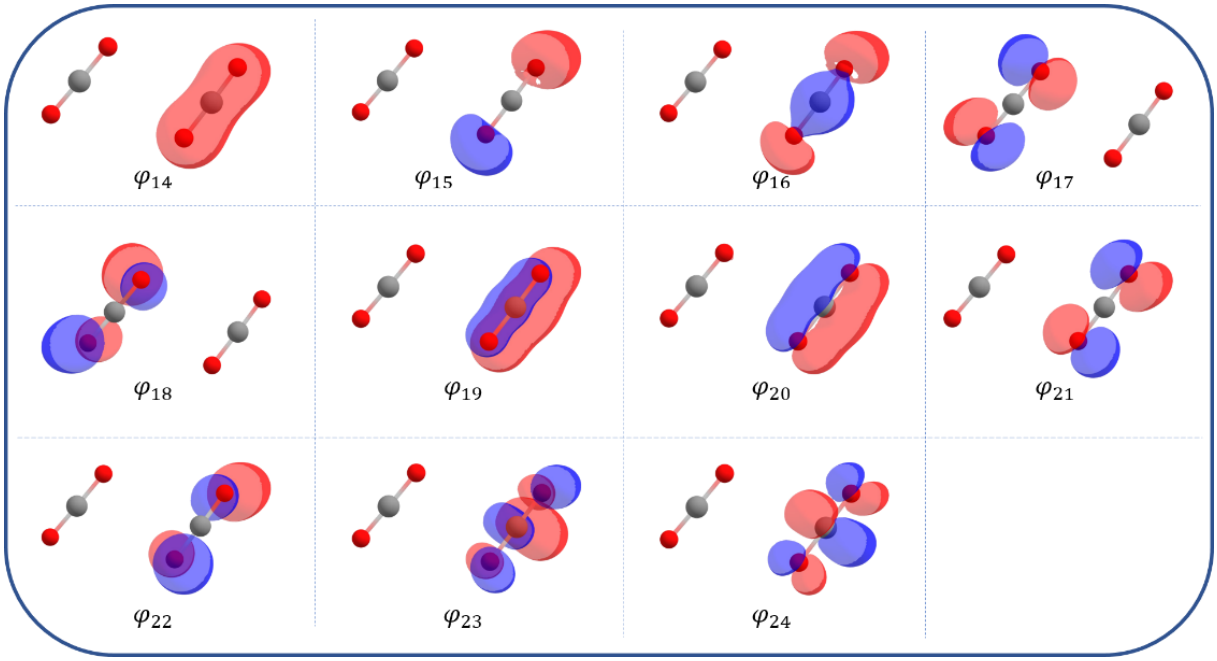

Supplementary Figure 7 Shows the 11 active XMS-CASPT2(17e11o) orbitals of $(CO_2)_2^+$ at the Franck-Condon (FC) geometry. Source data are provided as a Source Data file.

It is important to emphasize that we do not use any symmetry constraint or intentionally select localized vs. delocalized orbitals. The localization vs. delocalization of the active space orbitals is "spontaneous" and depends on the molecular geometry. Supplementary Figure 8 shows the six active XMS-CASPT2(7e6o) orbitals, calculated at the relaxed global minimum geometry of the $(CO_2)_2^+$ cation.

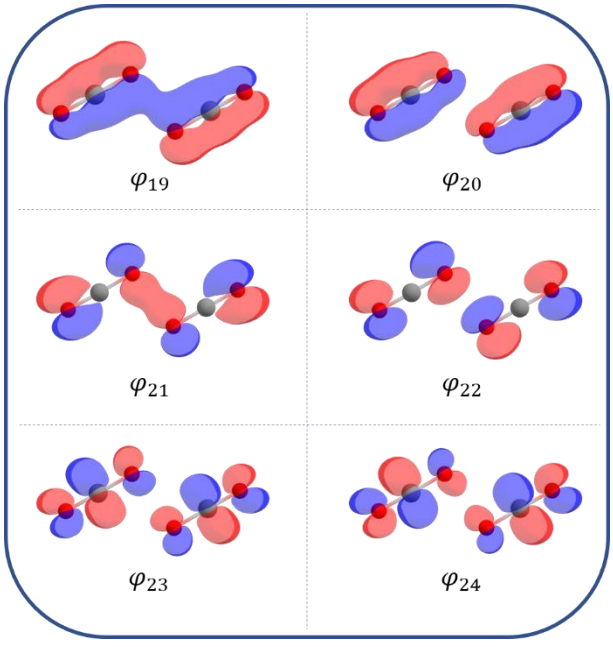

Supplementary Figure 8 Shows the six active XMS-CASPT2(7e6o) orbitals of $(CO_2)_2^+$ at the cation's global minimum (XMS-CASPT2 relaxed geometry). Source data are provided as a Source Data file.

The cartesian coordinates (Å) of the cation global minimum geometry are:

	Global cation minimum		
C	1.73	-0.06	0.00
O	2.68	0.61	0.00
O	0.75	-0.77	0.00
C	-1.73	0.05	0.00
O	-0.75	0.77	0.00
O	-2.68	-0.61	0.00